Electronic structure of the liquid 3d and 4d transition metals

1991 J. Phys.: Condens. Matter 3 4477

(http://iopscience.iop.org/0953-8984/3/24/016)

J. Phys.: Condens. Matter 3 (1991) 4477–4490. Printed in the UK

Electronic structure of the liquid 3d and 4d transition metals

W Jank, Ch Hausleitner and J Hafner

Institut für Theoretische Physik, TU Wien, Wiedner Hauptstraße 8-10, A-1040 Wien, Austria

Received 14 March 1991

Abstract. We present the first self-consistent calculation of the electronic density of states of the molten 3d and 4d transition metals. Our calculations are based on realistic models of the liquid structure and a linearized-muffin-tin-orbital supercell technique. We find that the electronic structure of transition metals undergoes only small changes on melting: the band width is almost the same, and the characteristic bonding–anti-bonding splitting of the d states is still observable in the liquid state. The theoretical predictions are compared with existing data on magnetic susceptibilities, x-ray, photoelectron and Auger-electron spectra.

1. Introduction

Today the structural and electronic properties of the liquid s–p bonded metals are well understood: diffraction experiments revealed the trends in the liquid structures [1] (which reflect rather closely those in the crystalline structures), photoemission investigations [2, 3] have established the trends in the electronic spectrum, and *ab-initio* calculations [4–7] have provided a clear picture of the physical mechanisms underlying these trends. On the other hand, the properties of the molten transition metals have been studied far less intensely and many of them are still rather poorly understood. This applies in particular to the electronic spectrum of molten transition metals. Experimental information remains fragmentary: an early work on the electronic density of states of liquid Cu using photoemission [8], a study of the d-electron density of states in liquid Fe, Co and Ni using soft x-ray emission and absorption spectroscopy [9], and some more recent work on *l*-Ni using Auger electron appearance potential spectroscopy [10] represent essentially all our direct information. Theoretical work is not much more advanced either. Progress has been hampered mainly for two reasons: (a) The hard-sphere model underlying most calculations can hardly be considered as a realistic representation of the structure of molten transiton metals. (b) Attempts to calculate the electronic spectrum have been based either on effective medium approximations [11–13] or real-space methods such as the recursion technique [14, 15] or momentum expansions [16, 17]. The effective medium approximations involve various approximations for decoupling the N-body correlation functions into the product of pair correlation functions. These are inadequate for describing the liquid structure and lead to unsatisfactory features in the electronic density of states. The real-space techniques use the full structural information (i.e. the coordinates of a given number

0953-8984/91/244477+14$03.50

of atoms rather than the pair correlation functions), but they are based on rather simplified tight-binding Hamiltonians involving a number of assumptions on the size and distance dependence of the interatomic transfer-integrals.

After the progress achieved in recent years, it seems now to be possible to return to the problem of the electronic structure of molten transition metals with a fair chance of success. First, it has been shown that the hybridized nearly-free-electron tight-binding (NFE–TB) approach to interatomic forces in transition metals originally introduced by Wills and Harrison [18] yields not only a simple and physically realistic description of transition metal cohesion, but leads via a molecular-dynamics simulation to liquid structure factors in quantitative agreement with diffraction data [19]. Second, progress in computational techniques and in computer performance has led to the development of various supercell techniques for calculating the electronic structure of liquid and amorphous metals self-consistently for realistic models of the atomic structure [4–6, 20, 21]. In favourable cases, even self-consistency of the atomic and electronic structure can be achieved by combining the Newtonian equations of motion of the molecular-dynamics with the formal equations of motion for the electronic degrees of freedom of the atoms within the supercell via the Hellmann–Feynman theorem [7, 22]. However, to date this ambitious approach can be made to work only within a plane wave basis, and this is inappropriate for the tight-bound d states of transition metals.

The approach to the electronic structure of molten transition metals presented here is thus based on the following strategy: (i) molecular-dynamics simulation of the liquid structure, based on NFE–TB potentials and (ii) a linear-muffin-tin-orbital (LMTO) supercell calculation of the electronic density of states. In section 2 we recapitulate very briefly the calculation of the interatomic potentials and the liquid structure. In section 3 we present the results of our linearized-muffin-tin-orbital (LMTO) calculations of the electronic structure for a range of molten 3d and 4d transition metals, and our conclusions are given in section 4.

2. Interatomic forces and liquid structures

2.1. Interatomic forces in transition metals

Our basic assumption is that the total energy of a transition metal may be decomposed into contributions from the s and d electrons. The s-electron contribution is treated in a NFE approximation, pseudopotential theory [23] is used to write the *s*-electron energy E_s as the sum of a volume energy and a pair interaction term. We use the local empty-core form of the pseudopotential (core radius R_c) [24] and the Ichimaru–Utsumi [25] local-field correction to the random-phase screening function.

The d-electron energy E_d may be written within a tight-binding-bond (TBB) approximation as the sum of a repulsive term and a bonding term, $E_d = E_{d-rep} + E_{d-bond}$ [18, 26–28]. The repulsive term may be parametrized in terms of a pair interaction provided by the electrostatic, exchange-correlation, and non-orthogonality contributions to the total energy [18, 26]. E_{d-bond} measures the covalent bond energy resulting from the formation of a d-electron band with the density of states $n(E)$. Quite generally, the covalent bond energy may be written as

$$E_{d-bond} = \frac{1}{2} \sum_{\substack{i,j \\ i \neq j}} h_{ij}(R_{ij}) \Theta_{ij} \tag{1}$$

where $h_{ij}(R_{ij})$ is the transfer integral and Θ_{ij} is the bond order which is defined as the difference between the number of electrons in the bonding $\frac{1}{\sqrt{2}}(\varphi_i+\varphi_j)$ and in the antibonding states $\frac{1}{\sqrt{2}}(\varphi_i-\varphi_j)$ (the indices i and j stand for the atomic site as well as for the orbital). If we assume the five d orbitals to be degenerate and use a Bethe lattice (or Cayley tree) as a reference system [19] for the calculation of the d-electron density of states and of the bond order, than we get a nearly semi-elliptic d-band DOS and the final result for the effective bonding pair-interaction $\Phi_{\mathrm{d-bond}}(R)=h(R)\Theta$ is equivalent, except for a sligthly different dependence of the bond order on the band filling, to that derived by Wills and Harrison [18] for a rectangular d band (see also Hausleitner *et al* [19]).

Finally hybridization between s and d states is taken into account by setting the numbers N_s and N_d of s and d electrons equal to the values resulting from a self-consistent band structure calculation for the crystalline transition metal.

The remaining parameters are determined as follows: $h(R)$ is the average canonical d–d transfer integral

$$h(R)=\tfrac{1}{5}[dd\sigma(R)^2+2dd\pi(R)^2+2dd\delta(R)^2]^{1/2}$$
$$h(R)=\frac{\sqrt{56}}{5}W_d\left(\frac{R_0}{R}\right)^5 \qquad (2)$$

where W_d is the width of the d band and R_0 is the nearest-neighbour distance in the crystal. W_d is the width of the d band from a self-consistent calculation for the crystalline metal. The core radius R_c of the s-electron pseudopotential is treated as an adjustable parameter chosen to get an accurate pair correlation function for the liquid and reasonable values for the pressure and compressibility (for a more detailed discussion, see [19]). The same value of R_c also yields reasonable phonon frequencies for the crystalline metals. The parameters for the 3d and 4d transition metals are given in table 1.

Table 1. Input parameters for the calculation of the interatomic forces: atomic volume V_{at}, numbers N_s and N_d of s and d electrons per atom, d-band width W_d, and s-electron pseudopotential radius R_c; see text.

	T (K)	V_{at} (Å^3)	N_s	N_d	W_d (eV)	R_c (Å)
Sc	1833	25.57	1.40	1.60	5.13	1.07
Ti	1973	19.17	1.39	2.61	6.08	1.06
V	2173	15.79	1.36	3.64	6.77	1.08
Cr	2173	13.77	1.42	4.58	6.56	0.94
Mn	1573	15.28	1.43	5.57	5.60	0.87
Fe	1833	13.23	1.42	6.58	4.82	0.80
Co	1823	12.71	1.43	7.57	4.35	0.69
Ni	1773	12.63	1.40	8.60	3.78	0.58
Y	1773	35.75	1.31	1.69	6.59	1.29
Zr	2173	25.55	1.30	2.70	8.37	1.29
Nb	2773	19.71	1.29	3.71	9.72	1.26
Mo	2880	17.04	1.45	4.55	9.98	1.07
Rh	2239	15.39	1.33	7.67	6.89	0.74
Pd	1823	16.83	1.21	8.79	5.40	0.53

As the only example we show in figure 1 (a) the effective pair interaction for liquid Pd (see [19] for more detailed results). This result illustrates rather nicely the physics of the transition metal bonding: the largest contribution to the binding energy comes from the covalent d–d bonding, around the nearest neighbour distance we have an equilibrium between the repulsive s and attractive d forces, at the scale of thermal energies ($\Phi - \Phi_{min} \simeq k_B T_M$, T_M is the melting temperature) the slope of the pair interaction is softer than for simple metals.

2.2. Liquid structure

Details of the calculation of the liquid structure using molecular-dynamics simulation, integral equations, and thermodynamic perturbation theory have been given in [19]. Liquid transition metals are rather a challenge to liquid state theory. TM interactions possess unique features: (a) extreme softness ('softness parameter' in a Weeks–Chandler–Andersen [29] expansion is $\xi \simeq 0.50$, compared to $\xi \simeq 0.44$ for a typical alkali metal and $\xi \simeq 0.40$ for Al) and (b) strong attractive minimum ($\Phi_{min} \simeq (3-5)k_B T_M$ for a transition metal, compared to $\Phi_{min} \simeq (0.5-1)k_B T_M$ for an alkali metal). As a result, the current liquid state theories are successful only for nearly complete d shells (Ni,Pd,...) and fail for the TM from the middle of the series where the covalent forces are strongest. Molecular dynamics (MD) simulations yield good agreement with diffraction data for all 4d and the 3d metals except Sc and Ti. Ti in particular has a somewhat anomalous structure factor, and the understanding of the interatomic forces and the liquid structure remains problematic. Note that such a problem does not exist for the 4d metals with a nearly empty d band (e.g., Y, Zr etc.) [19]. Two molecular dynamics simulations have been performed in parallel: (a) one for a large MD ensemble with $N = 1372$ atoms to produce reliable correlation functions and structure factors, and (b) one for a small ensemble with $N = 64$ particles in the periodically repeated cell to create the atomic coordinates for the electronic structure calculations. As the only example of our calculations, we show the results for liquid Pd. In figure 1(b), we compare the static structure factor with the diffraction data, in figure 1(c), we compare the pair correlation function calculated from 40 independent 1372-atom configurations with that determined from a single 64-atom configuration. As for the simple liquid metals and liquid semimetals [4–6, 30], we find that even a single 64-atom configuration is sufficient to grasp the main aspects of the liquid structure. A more complete compilation of the MD simulation results for the molten 3d metals and some of the 4d metals from the beginning of the series is given in [19].

3. Electronic structure

3.1. Computational aspects

Supercell calculations for the electronic structure of disordered materials may be performed either in a plane-wave basis or using a minimum basis set of localized orbitals. The advantage of a plane wave expansion is that it allows the use of the full atomic potential (or rather pseudopotential) and that the lowest eigenvalues of the very large Hamiltonian matrix may be calculated efficiently by dynamical simulated annealing techniques [6, 31], rather than by a repeated diagonalization of the Hamiltonian. The most convenient minimum basis set is given by linearized muffin-tin orbitals (LMTO

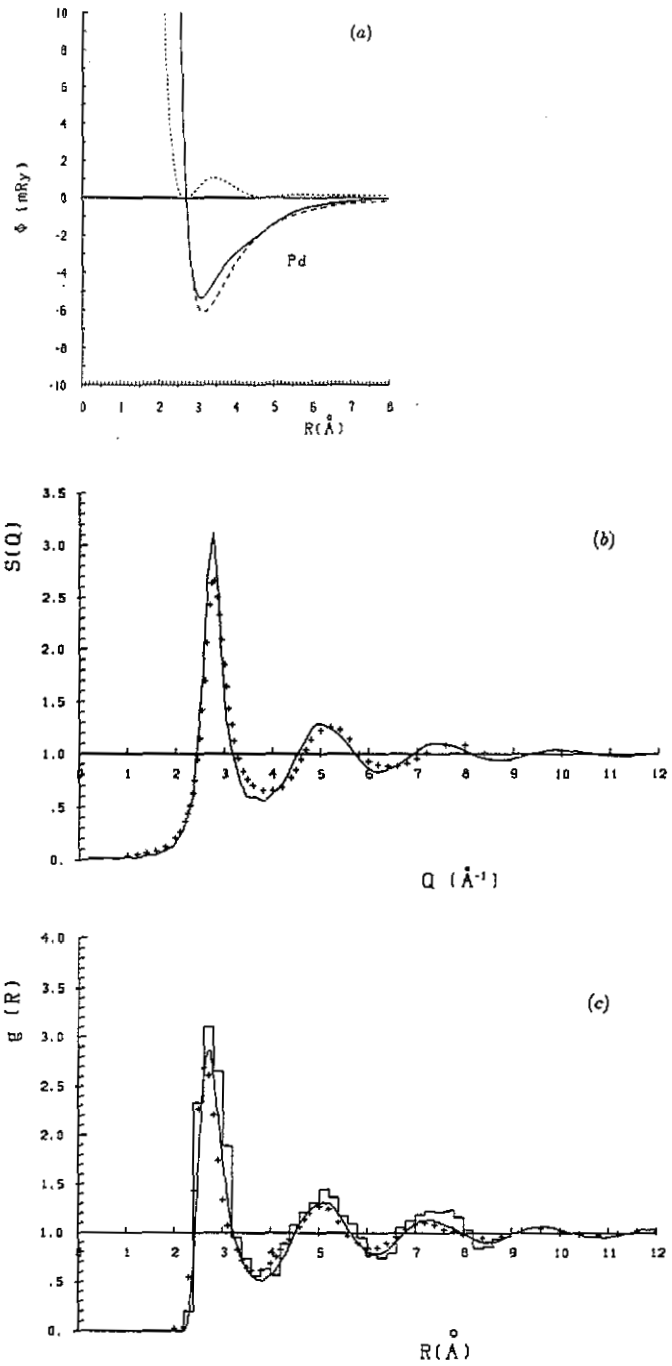

Figure 1. (*a*) Interatomic potential for liquid Pd. Full curve—total pair potential, broken curve—d-electron contribution; dotted curve—s-electron contribution. (*b*) Static structure factor of liquid Pd at $T = 1823$K. Full curve—MD simulation, crosses—experiment (after [1]). (*c*) Pair correlation function $g(R)$ for liquid Pd at $T = 1823$ K. Full curve—MD simulation (average over 40 independent configurations of a 1372-atom ensemble); histogram, MD simulation (pair correlation in one 64-atom configuration); crosses, experiment.

) in the atomic-sphere approximation ASA [32,33]. The disadvantage is the muffin tin form of the potential, the advantages are the small size of the Hamiltonian matrix (576 × 576 for a 64-atom cell) and the good convergence of the LMTO expansion even for the localized d orbitals of transition metals. Here we use the LMTO supercell technique. The technical aspects of the method have been discussed in [4]. Here we comment only briefly on the $\boldsymbol{k}$ point sampling necessary for the construction of the charge density and of the density of states (DOS) and on the ensemble averaging. Note that the supercell possesses the translational symmetry of the simple cubic lattice but not its point-group symmetry. During the self-consistency loop, the calculation has been done for a single special point ($\boldsymbol{k} = (0.25, 0.25, 0.25)\frac{\pi}{a}$) [34,35]; for the final DOS calculation a set of 32 $\boldsymbol{k}$ points (the stars of $\boldsymbol{k}_1 = (0.25, 0.25, 0.25)\frac{\pi}{a}$, $\boldsymbol{k}_2 = (0.25, 0.75, 0.25)\frac{\pi}{a}$, $\boldsymbol{k}_3 = (0.75, 0.75, 0.25)\frac{\pi}{a}$, $\boldsymbol{k}_4 = (0.75, 0.75, 0.75)\frac{\pi}{a}$)) has been used. The final DOS is obtained from the set of discrete eigenvalues using a Gaussian broadening (the width of the Gaussian is $\sigma = 0.3$ eV).

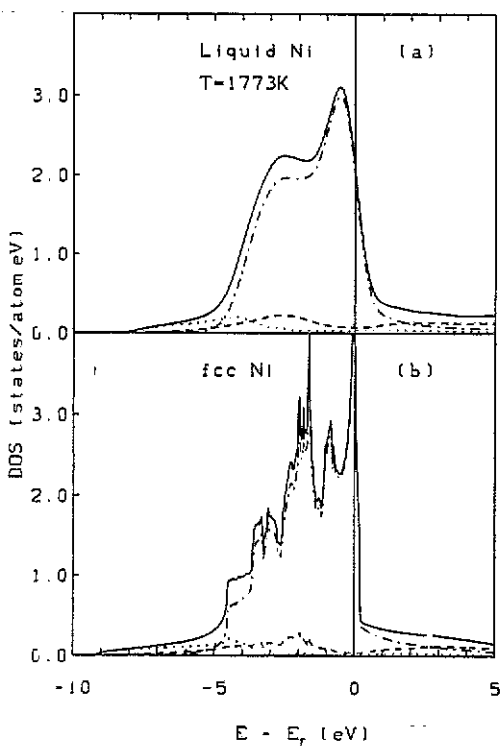

Figure 2. Electronic density of states in (*a*) liquid and (*b*) face-centred cubic Ni. Full curve, total DOS; dotted curve, s; broken curve, p; chain curve, d-electron contribution.

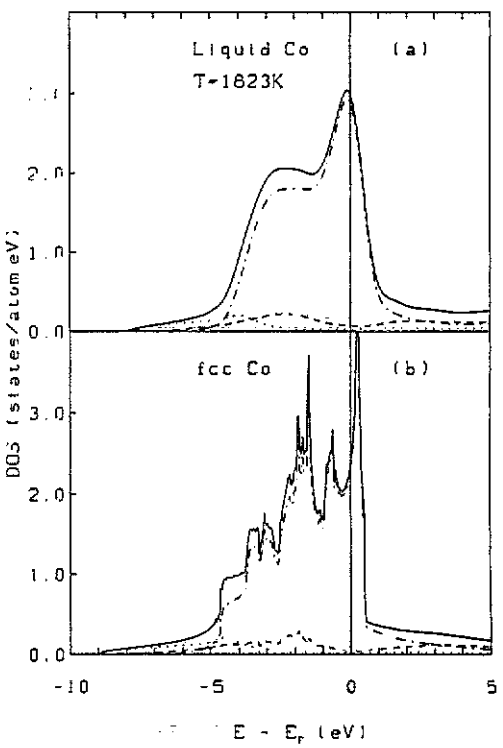

Figure 3. Electronic density of states (*a*) in liquid and (*b*) face-centred cubic Co. For key, see figure 2.

In principle, any physical property of a liquid should be calculated as an ensem-

ble average over a set of independent configurations. Already for the liquid simple metals we have found that the electronic DOS calculated for different configurations are very similar [4]; they are almost undistinguishable for the liquid transition metals. The majority of results presented below are thus based on a single representative configuration. Nevertheless, the selection of a representative configuration for a molten transition metal is a somewhat delicate problem. The width at half maximum of the first peak in the pair correlation function of a liquid transition metal is comparatively large ($\Delta R \simeq 20\%$ of the average nearest-neighbour distance) and the coupling integrals are strongly distance dependent ($\propto R^{-5}$ for d–d coupling). Hence, the existence of one or two pairs of atoms with a very short interatomic distance can lead to the formation of a resonant bound state below the bottom of the valence band. Since the effective pair interaction is strongly repulsive at short distances, such configurations and the bound states associated with them are extremely short-lived. Consequently, they are not representative of the overall electronic structure. They contribute only to a very flat band-tail at low energies. On the other hand, the existence of such bound states makes the approach to self-consistency extremely slow. For this reason, it is convenient (and acceptable) to select configurations without unusually short interatomic distances.

3.2. Electronic density of states

The electronic densities of states of liquid Cr, Mn, Fe, Co, and Ni, together with the DOS of the crystalline metals (obtained from a standard LMTO–ASA calculation and the tetrahedron method for the Brillouin zone integration [36], using 505 $\boldsymbol{k}$ points for the face-centered cubic and 506 $\boldsymbol{k}$ points for the body-centered cubic structure) are shown in figures 2 to 6. The results can be summarized as follows:

(*a*) The widths of the d bands (measured at a DOS of 0.5 (states/eV atom), i.e. just above the maximum s and p-DOS) are the same in the crystalline and in the molten state. A certain band narrowing expected because of the volume expansion is compensated for by a broadening of the bands arising from the fluctuations in the interatomic overlap integrals. In the series from Cr to Ni, the band width is reduced from $W_d = 6.2$ eV to $W_d = 4.4$ eV. This corresponds to the experimental observation obtained on the basis of the L_β-x-ray emission spectra [9] and contradicts any rigid band assumption [12]. That the band width is not changed upon melting is important for the calculation of the interatomic forces. Within our approximation, the pair interaction depends on the electronic structure via the width of the d band (the second moment of the DOS, respectively). The pair potential has been calculated for the band width of the crystalline metals. As the band width is the same in the molten metals, we can conclude that the liquid structure and the electronic structure are consistent at the level of the second moment.

(*b*) The DOS shows a remarkable similarity of the electronic structures of the crystalline and liquid metals. The characteristic bonding– antibonding splitting in the d band is clearly visible in the DOS of the melt. It is remarkable that the splitting is larger for the metals with a partially filled d band which crystallize in the bcc structure (Cr, Mn, Fe), and show a strong splitting in the crystalline DOS as well. No bonding–antibonding splitting has been predicted in earlier non-selfconsistent model calculations of the electronic structure [15]. The larger bonding–antibonding splitting in Cr, Mn, Fe produces the strong covalent bonding effects in elements with a nearly half-filled band. The splitting is also reflected in the strong attractive pair forces (see [19] and [37] for a more detailed presentation of the pair interactions).

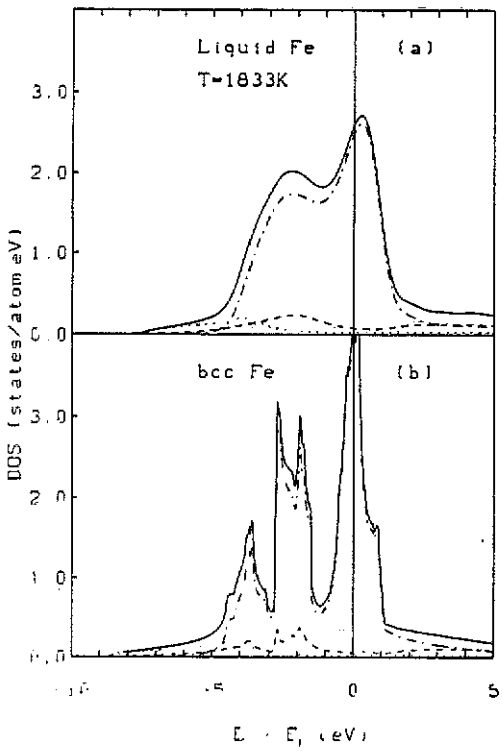

Figure 4. Electronic density of states in (*a*) liquid and (*b*) body-centred cubic Fe. For key, see figure 2.

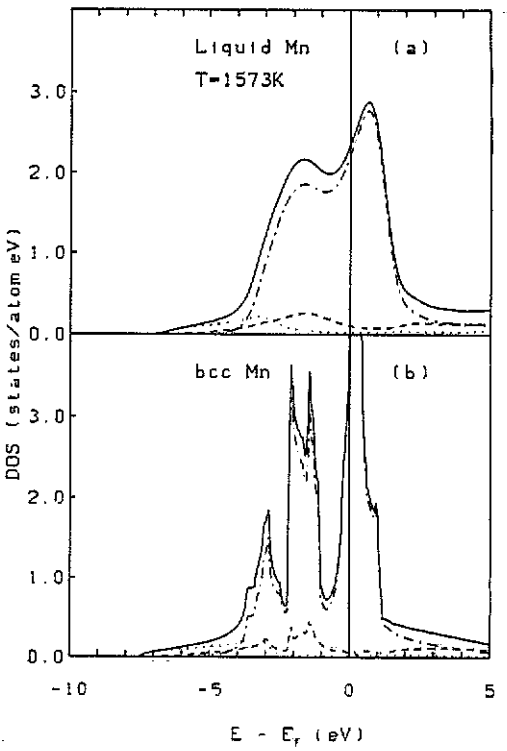

Figure 5. Electronic density of states in (*a*) liquid and (*b*) body-centred cubic Mn. For key, see figure 2.

No converging selfconsistent solution could be obtained for the 3d elements with a nearly empty d band (Sc, Ti, V). The origin of this difficulty is in the larger fluctuations in the local atomic environment (see also our remarks on the liquid structures in section 2.2 and in [19]).

No such difficulties exist for the 4d transition metals. The electronic DOS of all 4d elements (except for Tc and Ru, for which no liquid density data are available) are given in figure 7. The general trend is the same as in the 3d elements, except that the width of the d band is larger, due to the more extended nature of the 4d orbitals.

3.3. Comparison with experiment

3.3.1. Magnetic susceptibilities. In the Hartree–Fock approximation, the magnetic susceptibility per atom is related to the DOS at the Fermi level via

$$\chi = 2\mu_B^2 \left(\frac{n(E_F)}{1 - J_{\text{eff}} n(E_F)} \right) \tag{3}$$

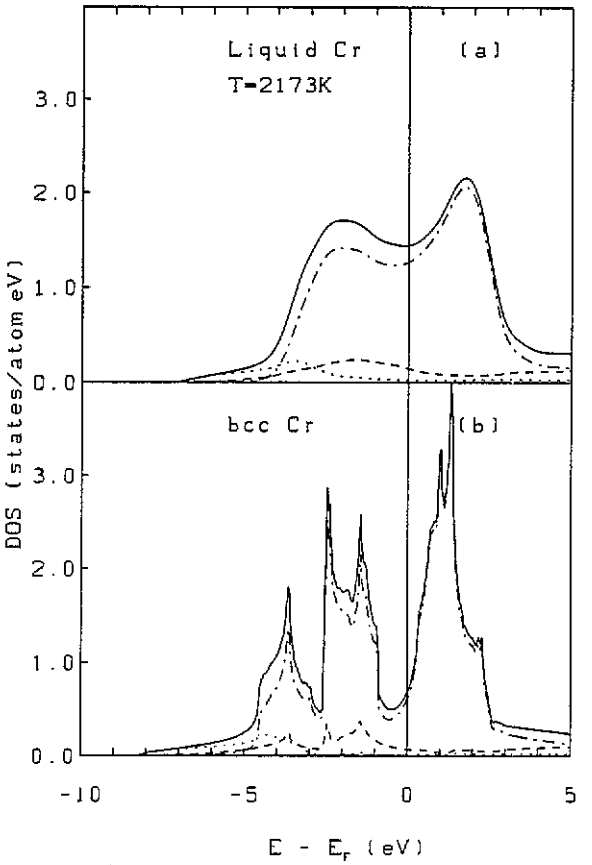

Figure 6. Electronic density of states in (*a*) liquid and (*b*) body-centered cubic Cr. For key, see figure 2.

where J_{eff} is the effective exchange interaction. We follow Asano and Yonezawa [12] and Asano and Yamashita [38] in setting $J_{\text{eff}} = 0.05$ and calculate the DOS at the Fermi level from the experimental susceptibilites of Busch *et al* [39, 40]. The data for some 3d elements are compiled in table 2 and show a good agreement between theory and experiment, with a maximum $n(E_F)$ for *l*-Co.

Table 2. Density of states at the Fermi level. Theory, as calculated in the supercell approach; experiment, as estimated from the magnetic susceptibilities [39, 40].

	$n(E_F)$ (states/eV atom)	
	Theory	Experiment
Ni	2.10	2.10
Co	2.99	2.95
Fe	2.59	2.60
Mn	2.34	2.40

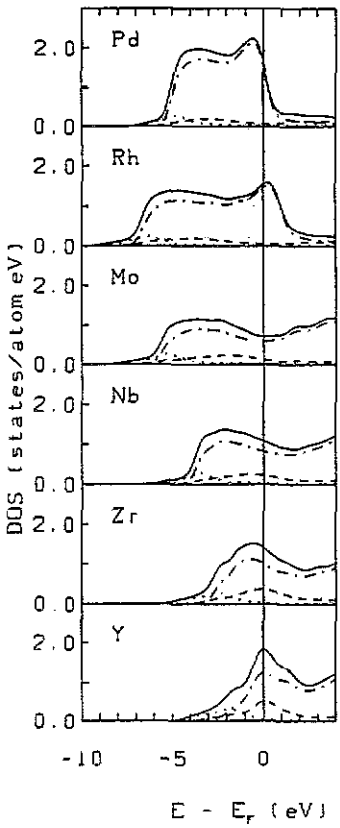

Figure 7. The electronic density of states in liquid 4d transition metals. For key, see figure 2.

3.3.2. Photoemission spectra. The most direct test of DOS calculations can be made via photoemission data, but any detailed comparison must consider the excitation and binding-energy dependence of the partial photoemission cross sections $\sigma_l(E, \hbar\omega)$. With the LMTO–ASA supercell technique, the $\sigma_l(E, \hbar\omega)$ may be calculated from the self-consistent potentials and the partial DOS in a single-scatterer final-state approximation and a dipole approximation for the photon field [41–43]. The calculated photoemission intensities

$$I(E, \hbar\omega) = \sum_l \sigma_l(E, \hbar\omega) n_l(E) \tag{4}$$

for the liquid 3d and 4d metals are shown in figures 8 and 9 for typical ultraviolet (UPS) and x-ray (XPS) excitation energies (the XPS spectrum has been Gaussian-broadened to account for the lower experimental resolution). Our results show that the partial photoionization cross sections $\sigma_l(E, \hbar\omega)$ depend quite strongly on the energy of the exciting photon, especially for elements with a nearly half-filled d band. Combined UPS and XPS measurements could thus provide a critical test of the theoretical predictions. Unfortunately, photoemission experiments have not been performed for liquid transition metals. Data are available only for a noble metal, Cu [8, 44]. For Cu, the experiment shows that only small modifications of the electronic structure occur at

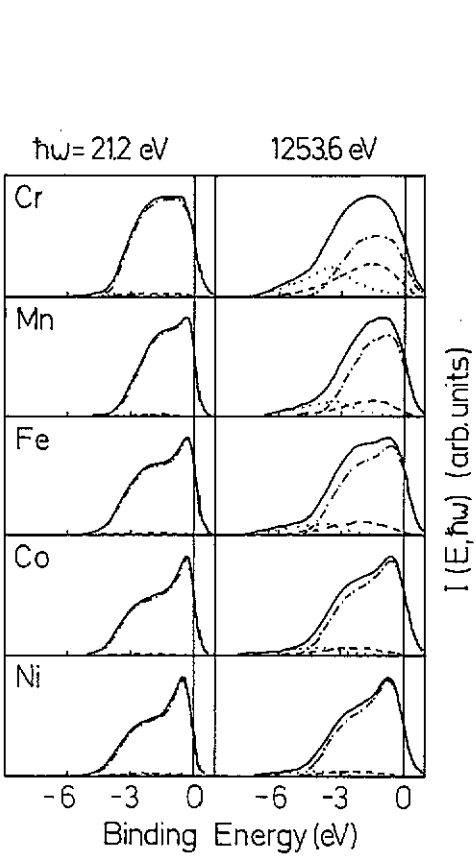

Figure 8. Photoemission intensities $I(E, \hbar\omega)$ of the liquid 3d metals, calculated for UPS and XPS excitation energies. Full curve, total intensity; dotted curve, s; broken curve, p; chain curve, d electron contribution.

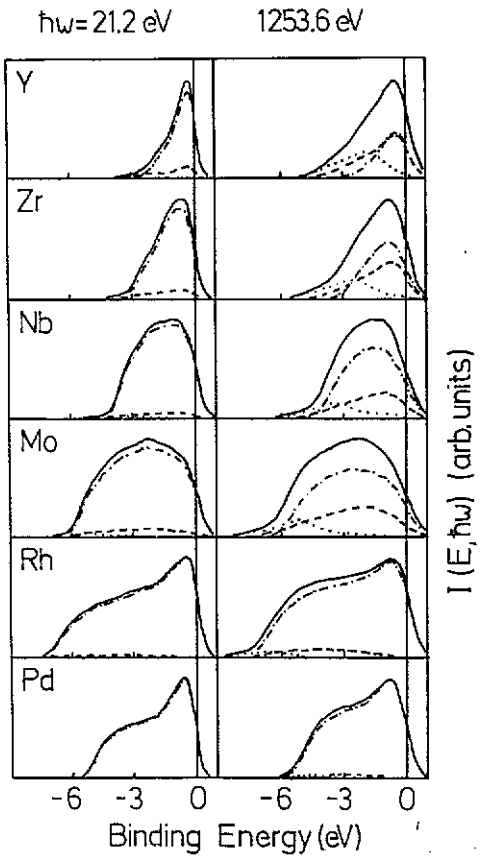

Figure 9. Photoemission intensities $I(E, \hbar\omega)$ of liquid 4d metals, calculated for UPS and XPS excitation energies. For key, see figure 8.

melting. If the transition metals behave in a similar way, this would tend to confirm our predictions. We hope that our work will stimulate new experiments.

3.3.3. Soft x-ray spectra. The L_β-x-ray emission and absorption bands reflects the partial DOS of the occupied and empty parts of the d band. Soft x-ray spectra (SXS) for liquid Fe, Co and Ni have been reported by Hague [9]. It should be noted that the resolution of SXS-spectra is limited by inner level broadening and the instrumental limit of resolution [45]. Figure 10 shows a comparison of the calculated d DOS, convoluted with a Lorentzian of width $\Gamma = 0.65$ eV (core-hole lifetime) and a Gaussian of width $\sigma = 0.5$ eV (instrumental broadening). Agreement between the theory and the experiment is reasonable, but evidently an experiment with such a limited resolution does not constitute a critical test of the shape of these rather narrow bands.

3.3.4. Auger appearance potential spectra. Dose *et al* [10] have used Auger electron appearance potential spectroscopy (AEAPS) to investigate the density of empty electronic states in solid and liquid Ni. According to the model of Park and Houston [46,

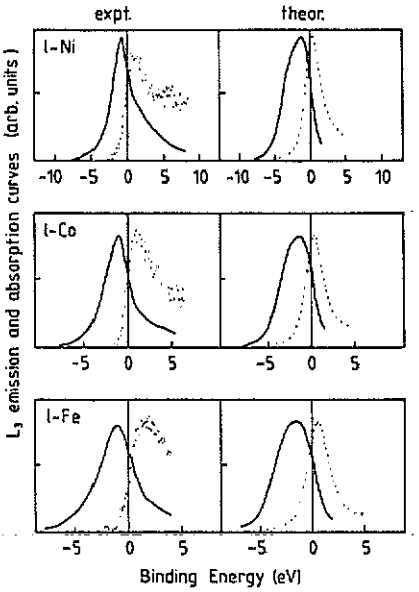

Figure 10. Theoretical and experimental L_3 emission (full curves) and self-absorption spectra (dotted curves) for liquid Fe, Co, and Ni. The experimental data were recorded at 2.5 kV (after Hague [9]).

47], the first derivative signal in AEAPS is given by an autoconvolution of the empty DOS (energies are measured relative to the Fermi level)

$$S(E) \sim \frac{\mathrm{d}}{\mathrm{d}E} \int_0^E N(E')N(E-E')\,\mathrm{d}E'. \tag{5}$$

Using equation (5) and accounting for core hole lifetime and instrumental broadening as described by Dose *et al* [10] (convolution with a Lorentzian of width $\Gamma = 0.4$ eV and a Gaussian of width $\sigma = 0.7$ eV), we calculate the spectrum shown in figure 11, which agrees favourably with experiment. The experiment clearly confirms the increase of the width of the empty part of the d band on melting (see also figure 2). The structures observed at 6 eV and 10 eV in c-Ni arise from the van Hove singularities in the crystalline DOS and disappear on melting. Otherwise the spectra undergo only small changes. In particular, we disagree with the conclusion of Dose *et al* [10] that the DOS at the Fermi energy *increases* on melting by a factor of 1.4. Their conclusion is based on a DOS derived via a complex deconvolution procedure. An increased DOS in the liquid would also be in direct contradiction to the observed and calculated decrease in the magnetic susceptibility (see section 3.3.1).

4. Conclusions

We have presented the first self-consistent calculation of the electronic DOS of the molten transition metals based on realistic models of the atomic structure. We find that the electronic structure of the transition metals undergoes only small changes on

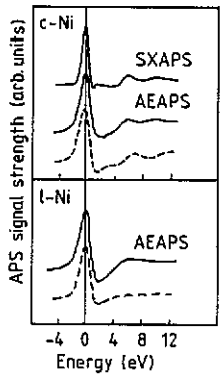

Figure 11. Auger and soft x-ray appearance potential spectra (AEAPS and SXAPS) for crystalline and liquid Ni. Full curve, experiment [10], broken curve, theory.

melting: the band width is essentially unaffected, the bonding–antibonding splitting of the d states is still observable in the molten state. We have attempted to make a critical assessment of our predictions against the available experimental information, and we hope that our results will stimulate further experiments.

Acknowledgments

This work has been supported by the Fonds zur Förderung der wissenschaftlichen Forschung in Österreich (Austrian Science Foundation) under project P7192-P and by the Bundesministerium für Wissenschaft und Forschung under contract No 49.658/3-II/A/4/90.

References

[1] Waseda Y 1980 *The Structure of Non-Crystalline Materials—Liquids and Amorphous Solids* (New York: McGraw-Hill)
[2] Indlekofer G, Oelhafen P, Lapka R, and Güntherodt H J 1988 *Z. Phys. Chem.* **157** 465
[3] Indlekofer G and Oelhafen P 1990 *J. Non-Cryst. Solids* **117/118** 340
[4] Jank W and Hafner J 1990 *Phys. Rev.* B **41** 1497
[5] Jank W and Hafner J 1990 *Phys. Rev.* B **42** 6926
[6] Hafner J and Jank W 1990 *Phys. Rev.* B **42** 11530
[7] Hafner J and Payne M C 1990 *J. Phys.: Condens. Matter* **2** 221
Stich I, Car R and Parinello M 1990 *Phys. Rev. Lett.* **63** 2240
[8] Williams G P and Norris C 1974 *J. Phys. F: Met. Phys.* **4** L175
[9] Hague C F 1977 *Liquid Metals 1976 (Inst. Phys. Conf. Ser. 30)* ed R Evans and D A Greenwood p 360
[10] Dose V, Drube R and Härtl A 1986 *Solid State Commun.* **57** 273
[11] Roth L M 1976 *J. Phys. F: Met. Phys.* **6** 2267
[12] Asano S and Yonezawa F 1980 *J. Phys. F: Met. Phys.* **10** 75
[13] Peters M A and Roth L M 1985 *J. Non-Cryst. Solids* **75** 455
[14] Haydock R, Heine V, and Kelly M J 1975 *J. Phys. C: Solid State Phys.* **5** 2845
[15] Fujiwara T 1979 *J. Phys. C: Solid State Phys.* **9** 2011
[16] Gaspard J P 1976 *AIP Conf.* **31** 372
[17] Khanna S N and Cyrot-Lackmann F 1978 *Philos. Mag.* B **38** 197
[18] Wills J H and Harrison W A 1983 *Phys. Rev.* B **28** 4363

[19] Hausleitner Ch, Kahl G and Hafner J 1991 *J. Phys.: Condens. Matter* **3** 1589
[20] Jaswal S S and Hafner J 1988 *Phys. Rev.* B **38** 7311
[21] Hafner J and Jaswal S S 1988 *Phys. Rev.* B **38** 7320
[22] Car R and Parinello M 1985 *Phys. Rev. Lett.* **55** 2471
[23] Heine V and Weaire D 1970 *Solid State Physics* vol 24 (New York: Academic) p 247
[24] Ashcroft N W 1966 *Phys. Lett.* **23** 48
[25] Ichimaru S and Utsumi K 1981 *Phys. Rev.* B **24** 7385
[26] Sutton A P, Finnis M W, Pettifor D G and Ohta Y 1988 *J. Phys. C: Solid State Phys.* **21** 35
[27] Pettifor D G and Podloucky R 1986 *J. Phys. C: Solid State Phys.* **19** 315
[28] Pettifor D G 1990 *Many Body Interactions in Solids* ed R M Nieminen, M J Puska and M J Manninen (Berlin: Springer) p 64
[29] Weeks J D, Chandler D, and Andersen H C 1971 *J. Chem. Phys.* **54** 5237
[30] Hafner J 1990 *J. Non-Cryst. Solids* **117/118** 18
[31] Payne M C, Bristow P D and Joannopoulus J D 1987 *Phys. Rev. Lett.* **58** 1348
[32] Andersen O K, Jepsen O, and Glötzel D 1985 *Highlights of Condensed Matter Theory* ed F Bassani, F Fumi, and M P Tosi (Amsterdam: North-Holland) p 59
[33] Skriver H L 1984 *The LMTO Method (Springer Series in Solid State Sciences 41)* (Berlin: Springer)
[34] Baldereschi A 1973 *Phys. Rev.* B **7** 5212
[35] Monkhorst H J and Pack J D 1976 *Phys. Rev.* B **13** 5188
[36] Lehmann G and Taut M 1972 *Phys. Status Solidi* b **54** 469
[37] Hausleitner Ch and Hafner J 1988 *J. Phys. F: Met. Phys.* **18** 1025
[38] Asano S and Yamashita J 1973 *Prog. Theor. Phys.* **49** 373
[39] Busch G, Güntherodt H J, Künzi H U and Meier H A 1973 *The Properties of Liquid Metals* ed S Takeuchi (London: Taylor and Francis) p 263
[40] Busch G and Güntherodt H J 1974 *Solid State Physics* vol 29 (New York: Academic) p 235
[41] Jarlborg T and Nilson 1979 *J. Phys. C: Solid State Phys.* **12** 265
[42] Redinger J, Marksteiner P and Weinberger P 1986 *Z. Phys.* B **63** 321
[43] Jank W and Hafner J 1990 *J. Phys.: Condens. Matter* **2** 5065
[44] Norris C 1977 *Liquid Metals 1976 (Inst. Phys. Conf. Ser. 30)* ed R Evans and D A Greenwood p 171
[45] Hague C F, Fairlie R H, Temmermann W M, Gyorffy B L, Oelhafen P, and Güntherodt H J 1981 *J. Phys. F: Met. Phys.* **11** L95
[46] Houston J E and Park R L 1972 *Phys. Rev.* B **5** 3808
[47] Park R L and Houston J E 1972 *Phys. Rev.* B **6** 1073